SUBDUCTED BASALTS AND SEDIMENTS AS SOURCES FOR FELSIC DYKES IN THE MAWAT OPHIOLITE, NE IRAQ

Heider Al Humadi*,,✉, Markku Väisänen*, Sabah A. Ismail***, Marja Lehtonen°** and **Bo Johanson°**

** Department of Geography and Geology, 20014 University of Turku, Finland.*
*** Department of Applied Geology, College of Sciences, University of Babylon, Iraq.*
**** Department of Applied Geology, College of Sciences, University of Kirkuk, Iraq.*
° Geological Survey of Finland, 0251 Espoo, Finland.
✉ Corresponding author, email: heialm@utu.fi

Keywords: *tonalites; granites; adakites; fractionation; mixing; Mawat ophiolite; Zagros.*

ABSTRACT

The Mawat ophiolite is a fragment from the Neo-Tethyan oceanic lithosphere and is considered as the largest and best-exposed ophiolite within the Zagros Suture Zone, northeast Iraq. Felsic dykes are encountered in three locations in the Mawat ophiolite. Here, we use field work, petrology and geochemical data to investigate the magma sources of the felsic dykes. The felsic dykes are classified into two types: oceanic plagiogranites in the western (Mirza and Ismail, 2007) and leucogranites in the central (Mohammad et al., 2014) Mawat ophiolite, here called tonalites and granites, respectively. Both types, mixed in various proportions occur in the eastern felsic dykes. The eastern tonalites are weakly peraluminous to metaluminous and are low in K_2O (0.13-0.24 wt%) and TiO_2 (0.01-0.07 wt%) and high in Na_2O (6.63-11.02 wt%). The eastern granites are strongly peraluminous, moderate to high in K_2O (1.16-6.57 wt%) and Na_2O (2.83-6.47 wt%), and very low in TiO_2 (0.03-0.07 wt%). The western tonalites are similar to adakites and are interpreted to have crystallized from melts of subducted oceanic crust interacting with the mantle. The eastern tonalites underwent hornblende and plagioclase fractionation in shallow-level magma chambers modifying their original compositions. The granites are interpreted to derive from melting of psammitic sediments on top of the subducted slab. Parental melts of the tonalities and granites were partially mixed in shallow magma chambers in eastern Mawat.

INTRODUCTION

Small volumes of felsic magmatic rocks are commonly associated with modern oceanic crust and ancient ophiolites. They occur as metre- to kilometre-scale dykes and intrusive bodies in the upper portion of the lower oceanic crust. They are particularly abundant in the upper gabbros and in the root zones of the sheeted dyke complexes in ophiolites (e.g. Coleman and Peterman, 1975; Flagler and Spray, 1991; Amri et al., 1996; Koepke et al., 2007; France et al., 2009).

These rocks are composed of plagioclase and quartz, minor ferromagnesian minerals and rare K-feldspar with very low K_2O contents (~ 0.2 %; Coleman and Peterman, 1975; Amri et al., 1996; Koepke et al., 2007; Dilek and Furnes, 2014; 2017) and have compositions corresponding to diorite, quartz diorite, tonalite, trondhjemite and albite-anorthosite (Amri et al., 1996; Li and Li, 2003; Li et al., 2008; Meffre et al., 2012; Freund et al., 2014). They are commonly referred to as oceanic plagiogranites. Another type of felsic rocks identified in several ophiolites is composed of K-feldspar, plagioclase, quartz and mafic mineral forming up to 5% (Pearce, 1989). These are often called leucogranites.

Different magmatic processes leading to the formation of felsic rocks in ophiolites have been recognized: i) fractional crystallization of basaltic magmas at shallow depths (Coleman and Peterman, 1975; Amri et al., 1996; Floyd et al., 1998; Freund et al., 2014), ii) partial melting of hydrated mafic (Malpas, 1979; Gerlach et al., 1981; Flagler and Spary, 1991; Keopke et al., 2004; Grimes et al., 2013) and sedimentary rocks (Haase et al., 2015; Rollinson, 2015), iii) liquid immiscibility (Dixon and Rutherford, 1979; Ulrich and Borsien, 1996).

Studies on felsic rocks in ophiolites have shown that they may form at different stages of the evolution, from mid-ocean ridge through spreading, subduction and obduction leading to a variety of felsic rocks observed in ophiolites (Searle and Malpas, 1980; Pedersen and Malpas, 1984; Pearce, 1989; Flagler and Spary, 1991; Amri et al., 1996; Whitehead et al., 2000; Li and Li, 2003; France et al., 2010; Dilek and Furnes, 2014; Santosh et al., 2016).

Small volumes of felsic dykes occur in the central and western Mawat ophiolite (MO), NE Iraq, intruded into the upper mantle peridotite (Mohammad et al., 2014; Mohammad and Qaradaghi, 2016) and crustal gabbros (Mirza and Ismail, 2007). Similar rocks have been reported in other ophiolitic sequences, e.g., Kizildag (Dilek and Delaloye, 1992), Oman (Rollinson, 2014; 2015), Neyriz (Moghadam et al., 2014), New Caledonia (Maurizot et al., 2020), and Pushtashan ophiolites (Ismail et al., 2017).

In this study, we describe geochemistry and petrography of felsic dykes recently found in the eastern MO and discuss their magma sources and regions. Our findings will be discussed in comparison with felsic intrusions from the western (Mirza and Ismail, 2007) and central (Mohammad et al., 2014) MO.

REGIONAL GEOLOGY

The MO is located within the Iraq Zagros Suture Zone (IZSZ) of northeast Iraq, about 30 km northeast of the city of Sulaimani (Figs, 1 and 2). The IZSZ is part of the 2000 km long Zagros-Bitlis Suture Zone, which extends from southeastern Turkey through northern Syria and Iraq to western and southern Iran (Dilek and Moores, 1990; Dilek et al.

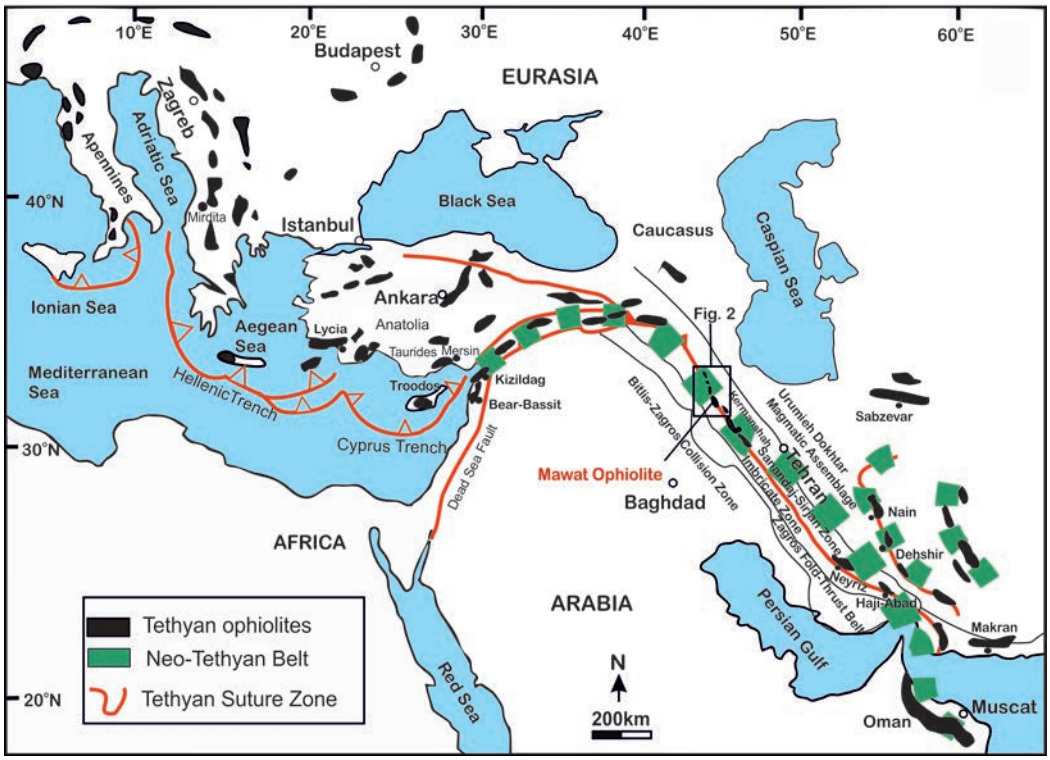

Fig. 1 - Distribution of Tethyan ophiolites and suture zones in the eastern Mediterranean and the Zagros Orogenic Belt (modified from Dilek et al., 2007). Tectonic units modified from Alavi (2008).

2007; Dilek and Thy, 2009; Fig. 1). The Zagros-Bitlis Suture Zone was formed by closure of the Neo-Tethys Ocean, during the progressive Mesozoic to present collision between the Arabian and the Eurasian continents (Alavi, 1980; Agard et al., 2005; Mouthereau, et al., 2012; Koshnaw et al., 2019). Fragmented ophiolite remnants mark the boundary between the Arabian and the Eurasian continental margins (Dilek and Furnes, 2019; Fig. 1) providing geological continuity between the ophiolites in the Turkish Taurides and those from the Zagros in Iran. The ophiolites in the IZSZ are classified in terms of age in Late Cretaceous and Paleogene (Ismail and Carr, 2008; Ismail et. al., 2014).

The IZSZ is composed of three units, i.e. Qulqula-Khwakurk, Penjwen-Walash and Shalair units (Buday and Jassim, 1987; Jassim and Goff, 2006; Fig. 2). The Penjwen-Walash unit consists of two thrust sheets: the lower allochthon is the Eocene-Oligocene Walash-Naopurdan Group, made up of volcanic-sedimentary arc rocks (Ali et al., 2013), and the upper allochthon is the Cretaceous Gimo-Qandil Group, which represents the ophiolite-bearing terrane (Ali et al., 2012). Both allochthons rest on the Arabian plate margin above the Red Beds and radiolarian cherts. The upper allochthon contains Cretaceous ophiolites and supra-subduction zone complexes that include the Mawat, Penjwen and Pushtashan ophiolites (Ismail et al. 2014; 2017; 2020). The lower allochthon includes fragments of mélange-type ophiolites of Rayat (Arai et al., 2006; Ismail et al., 2009) and Qalander (Ismail and Al-Chalabi, 2006).

GEOLOGY OF THE MAWAT OPHIOLITE AND ITS FELSIC DYKES

The MO is one of the largest and best-exposed fragment of oceanic lithosphere within the IZSZ (Jassim, 1973; Al-Mehaidi, 1974). The MO is well-preserved and consists of mantle peridotites and thick crustal gabbros intruded by minor diorites and diabase dykes. Volcanic rocks were also observed (Fig. 3). Layered and amphibole-rich gabbros are the main components of the crustal sequence and form two-thirds of the complex. The volcanic rocks are divided into two units: the lower metavolcanic unit (the Mawat group) and the upper volcano-sedimentary unit (the Gimo group). These units are exposed in the northern and southern parts of the MO. The thickness of these units is about 600 metres and they are composed of alternating white siliceous carbonate and dark calcschists with thin metavolcanic interlayers. The contacts between these three rock units are thrust faults (Mirza and Ismail, 2007; Ismail et al., 2010; Mohammad et al., 2014, Mohammad and Qaradaghi, 2016; Mohammad and Cornell, 2017; Fig. 3). The mantle peridotites are intruded by numerous pyroxenite dykes and tectonically overlie the mafic rocks. The uppermost part of the MO is overlain by the volcanic and sedimentary rocks of the Gimo group in the north. In the east, west, and south, the MO rocks are sandwiched between two thrust sheets of Walsh and Naopurdan groups and in turn, the MO and Walah-Naopurdan volcanic rocks are thrust over the Tertiary Red beds (Fig. 3). The MO rocks and the Gimo sequences underwent low-grade metamorphism (Jassim and Goff, 2006).

A previous study has found felsic dykes within the gabbroic rocks in the western part of the MO. The dyke samples are white to light grey in colour, medium- to coarse-grained and vary in width from few centimetres to few metres. They are composed of quartz, plagioclase and rare K-feldspar (Mirza and Ismail, 2007).

In the central part of the MO. near the village of Daraban, NW-SE trending 1-20 m wide felsic dykes occur within harzburgites (Mohammad et al., 2014). The dykes are white in colour with coarse-grained texture and they are composed of quartz, K-feldspar, plagioclase, muscovite and tourmaline. The Daraban granite yields an age of 96.8±6.0 Ma (U-Pb

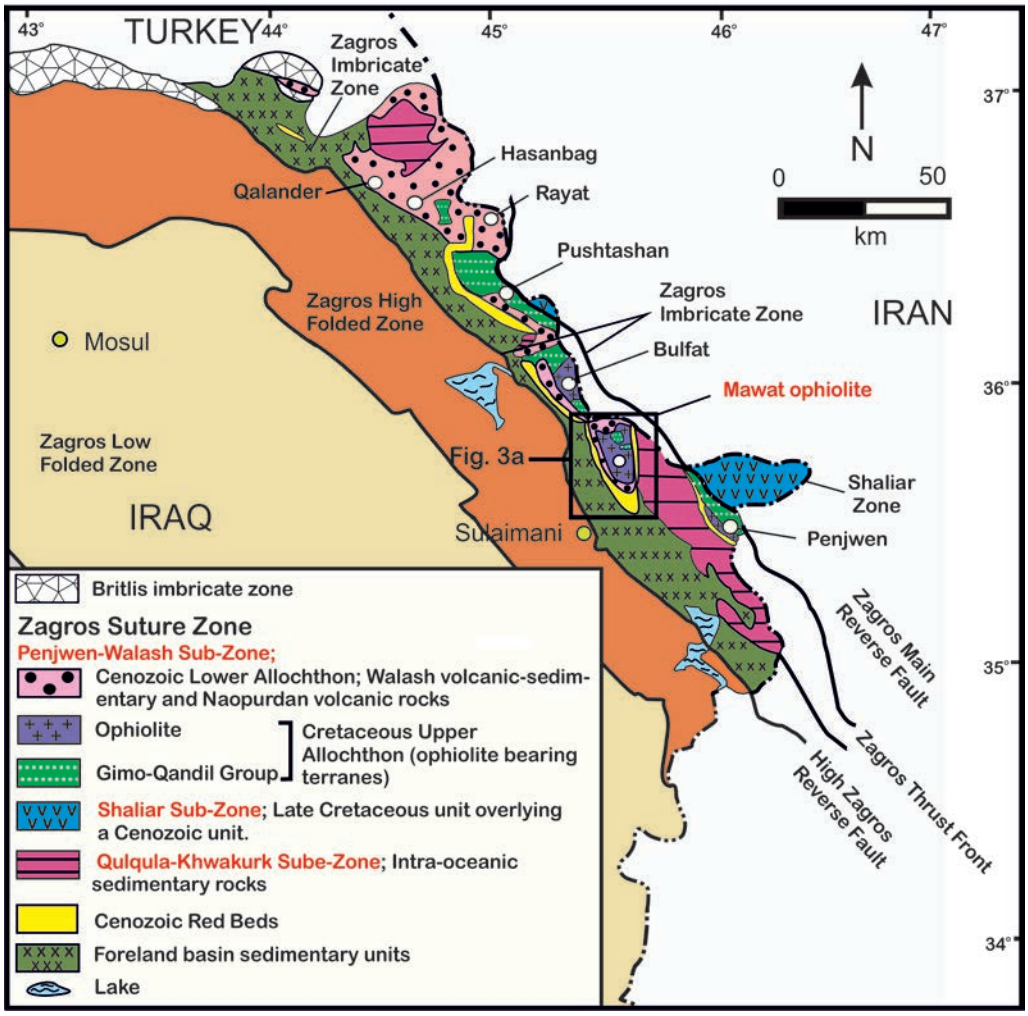

Fig. 2 - Regional tectonic map of NE Iraq Kurdistan region showing the major tectonic subdivisions, modified from Al-Kadhimi et al. (1996). Tectonic zones and boundaries modified from Al-Qayim et al. (2012).

zircon; Mohammad and Qaradaghi, 2016) and 93.4±1.8 Ma (Rb/Sr mineral isochron; Azizi et al., 2013).

In this study we focus on eight felsic dykes that were recently discovered in the eastern part of the MO. They occur as a series of NW-SE striking 3-35 m wide dykes with unknown lengths in the upper part of the mantle section (Figs. 3a, b and 4). Some of the narrow dykes show chilled margins. Gradational contact with the wall rocks (dunite and serpentinized harzburgite) is observed in a single narrow dyke. One of the dykes yields an age of 94.6±1.2 Ma (U-Pb monazite; Al Humadi et al., 2019).

ANALYTICAL METHODS

Eight samples were analysed at Acme Analytical Laboratories Ltd. (Acme) in Vancouver, Canada. The samples were pulverized in a mild steel swing mill and after the $LiBO_2$ fusion and HNO_3 dilution, the major elements, Cr, and Sc were analysed by inductively coupled plasma-emission spectrometry (ICP-OES) with Spectro Ciros Vision instrument. The other trace elements were analysed by inductively coupled plasma-mass spectrometry (ICP-MS) with PerkinElmer ELAN 9000 instrument. The analytical precision is 1-5% for the major oxides and ±10% for the other elements. More detailed descriptions can be found at http://acmelab.com/services/downloads/. The data are analysed and plotted using GCDKit software (Janousek et al., 2006). The geochemical data are presented in Table 1.

To support the optical mineralogy, two analytical methods were used. The element mapping was done with Bruker M4 Tornado micro-XRF facility equipped with two SDD detectors at the University of Turku, Finland. The spot size of mapping was 20 μm, step length 40 μm and the analysis time per pixel was 16 ms. More detailed mineral identification with point analysis was performed in the Finnish Geosciences Research Laboratory at the Geological Survey of Finland, Espoo with Hitachi SU3900 scanning electron microscope, with Oxford Instruments' energy dispersive spectrometer (EDS) equipped with a 20 mm^2 ultra-thin window. Prior to analysis the thin sections were carbon coated. The analyses were performed in high vacuum at an accelerating voltage of 20kV and a probe current of 1 nA, with a live time measuring time of 15 s. The analysis platform used was INCA (Oxford Instruments). The detector was optimized using a Cu standard prior to analysis. All analyses were normalized to 100 w% after performing ZAF matrix correction procedures.

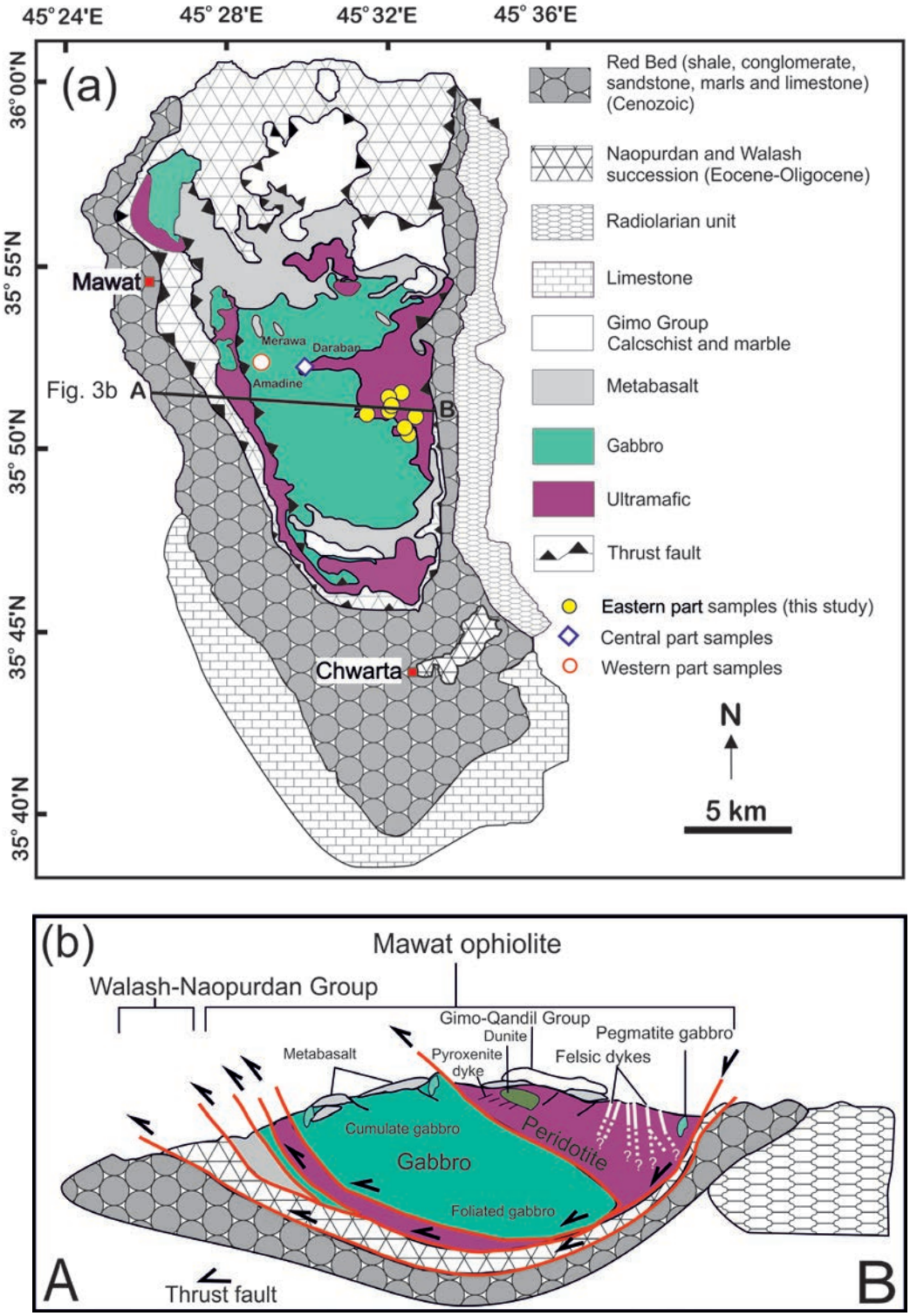

Fig. 3 - a) Simplified geological map of the Mawat ophiolite, modified from Aziz (2008). b) Simplified cross-section of the Mawat ophiolite along the traverse A-B, modified from Al-Qayim et al. (2012). For location and legend, see Fig. 3a.

RESULTS

Petrography

Two types of felsic samples were recognized. Type-1 samples are medium- to coarse-grained with hypidiomorphic, porphyric and, rarely, myrmekitic and granophyric textures. These rocks are composed of plagioclase, amphibole, quartz, and very rare biotite, muscovite and K-feldspar (Fig. 5a-c). Apatite, epidote, titanite, zircon, monazite, ilmenite and magnetite are accessory minerals. The subhedral to anhedral plagioclase is albite which is the dominant mineral partially altered to sericite. The intergrowth of quartz and albite is expressed in granophyric texture and some of the albite phenocrysts contain fine-grained quartz and plagioclase inclusions. The plagioclase laths form the framework with interstitial spaces filled by quartz, hornblende and rare muscovite, biotite and chlorite. The mafic phases are mainly hornblendes but two grains contain low concentrations of Ti. They occur as needles or fibrous crystals in a radial shape, and they crystallized at the rims of the albite phenocrysts (Fig. 5a and b), which suggests a secondary origin. A few hornblendes have partly altered into biotite. Hereafter, these samples are referred to as tonalites.

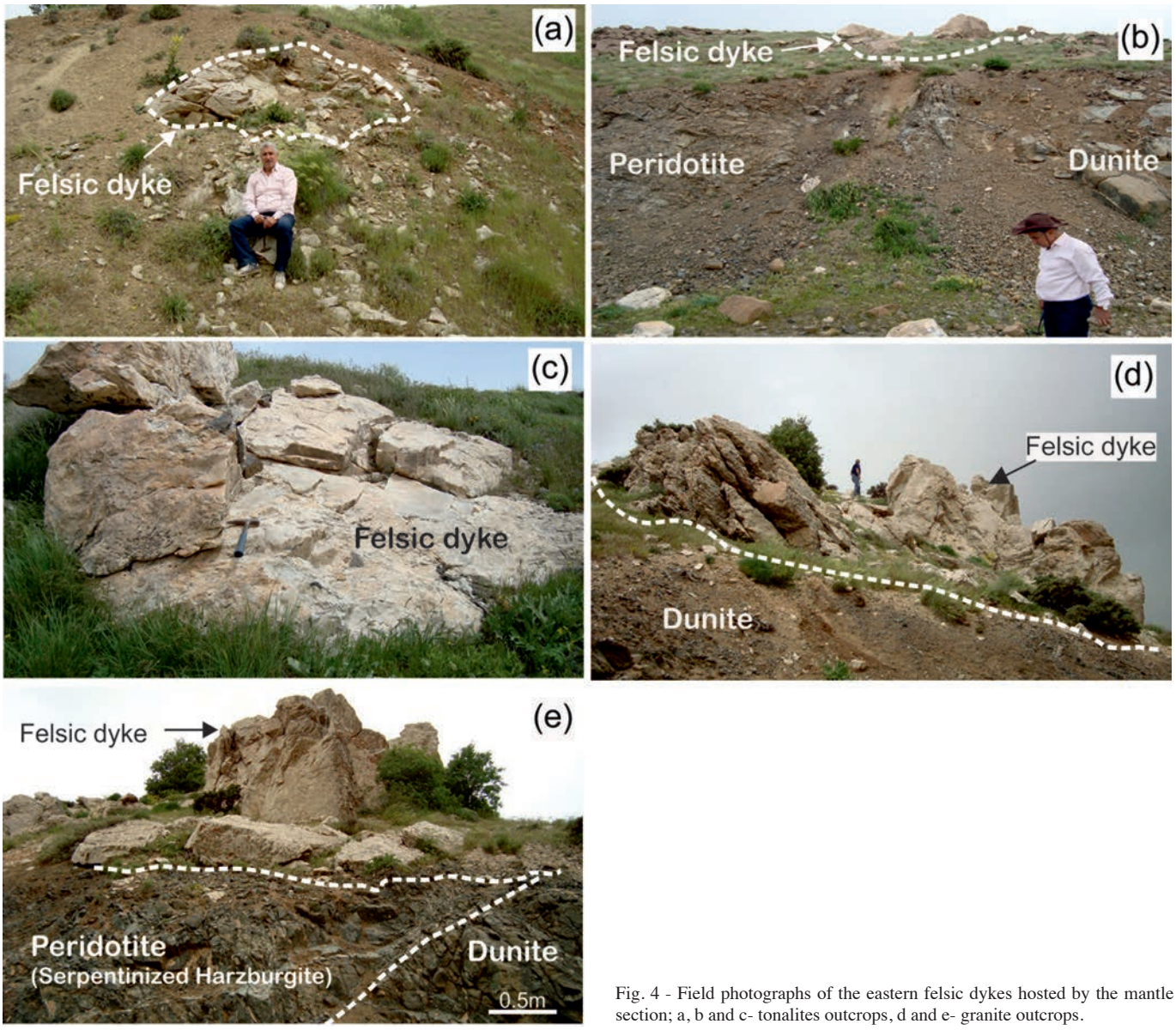

Fig. 4 - Field photographs of the eastern felsic dykes hosted by the mantle section; a, b and c- tonalites outcrops, d and e- granite outcrops.

Type-2 samples are medium- to coarse-grained and white to pale grey in colour. They are composed of K-feldspar, quartz, plagioclase, muscovite, and biotite with or without tourmaline (Fig. 5d-f). Accessory minerals are apatite, zircon, monazite, xenotime, ilmenite, titanite and magnetite. The subhedral to anhedral feldspars are characterized by large crystals, occasionally yielding porphyritic textures. Myrmekitic, perthitic and microperthitic textures are also found. Up to 2.5 cm crystals of tourmaline were observed in sample D3/G and up to 25 cm were locally found. The plagioclase is albite which is partially altered to sericite. Some plagioclase show kinked twins (Fig. 5e). The quartz grains display undulose extinction and re-crystallisation through sub-grain formation (Fig. 5d). The K-feldspar phenocrysts in samples 17G and D3/G are veined by a network of late-stage fine-grained quartz (Fig. 5j). The quartz veinlets occur within the cleavage planes of the deformed feldspars. A few muscovites are slightly folded. Inclusions of plagioclase, quartz, muscovite, biotite minerals can be observed within the feldspar phenocrysts (Fig. 5f). Hereafter, these samples are referred to as granites.

Geochemistry

Major elements

Type-1 samples (Table 1; Fig. 7) have SiO_2 contents from 64.93 to 74.22 wt%, low TiO_2 (< 0.07 wt%) and CaO (0.24 to 1.72 wt%), and low to high Al_2O_3 (12.48 to 20.77 wt%) contents. They are enriched in Na_2O (6.63 to 11.02 wt%) and depleted in K_2O (0.13 to 0.24 wt%). In the Total Alkalis vs. Silica (TAS) diagram they plot in the granite and quartz monzonite-syenite fields (Fig. 6a). They are weakly peraluminous with Alumina Saturation Index (ASI) values between 1.02 and 1.04, but sample 23G is metaluminous with ASI value of 0.97 (Fig. 6b). The samples from western Mawat (Mirza and Ismail, 2007) plot in the same fields as the Type-1 samples of this study. The eastern tonalites have lower MgO contents compared to the western ones (Fig. 7a). However, Mg# in both locations are similar (Fig. 7g).

Type-2 samples (Table 1; Fig. 7) have high SiO_2 contents (74.82 - 76.25 wt%) and low TiO_2 (0.03 - 0.07 wt%), high Na_2O (6.36 - 6.47 wt%) except sample 17G (2.83 wt%), as well as moderate to high K_2O (1.16 - 6.57 wt%) and low

Table 1 - Major (wt%) and trace element (ppm) analyses of felsic rocks from the eastern Mawat ophiolite.

Sample	17G	21GS	22GCO	D3/G	15G	18G	19G	23G
Locality	Rashakani	Shakarout	Shakarout	Top of Ser Shiw	Rashakani	Shakarout	Shakarout	Waraz
Rock Type	granite	granite	granite	granite	tonalite	tonalite	tonalite	tonalite
N-Coord	35° 51. 24'	35° 51. 29'	35° 51. 28'	35° 51. 24'	35° 52. 21'	35° 51. 24'	35° 50. 41'	35° 50. 39'
E-Coord	45° 32. 56'	45° 31. 11'	45° 32. 11'	45° 32. 55'	45° 32. 53'	45° 32. 60'	45° 33. 12'	45° 33. 11'
SiO_2	74.82	75.66	76.25	76.16	74.05	66.99	64.93	74.22
TiO_2	0.06	0.07	0.07	0.03	0.07	0.01	0.02	0.04
Al_2O_3	14.07	14.34	13.7	14.07	15.18	19.18	20.77	12.48
Cr_2O_3	<0.002	<0.002	<0.002	<0.002	<0.002	<0.002	<0.002	<0.002
Fe_2O_3	0.75	0.69	0.51	0.65	0.79	0.52	0.55	1.72
FeO	0.67	0.62	0.45	0.58	0.71	0.46	0.49	1.54
MgO	0.15	0.28	0.23	0.17	0.22	0.59	0.44	2.62
CaO	0.14	0.61	0.45	0.42	0.73	0.24	1.72	1
Na_2O	2.83	6.36	6.37	6.47	8.03	11.02	10.33	6.63
K_2O	6.57	1.16	1.61	2.05	0.16	0.24	0.13	0.14
P_2O_5	0.05	0.05	0.06	0.08	0.11	0.05	0.01	0.04
MnO	0.01	<0.01	<0.01	0.01	<0.01	<0.01	<0.01	0.02
LOI	0.5	0.8	0.7	-0.2	0.6	1.1	0.7	1
Sum	99.98	99.97	99.97	99.91	99.97	99.95	99.64	99.92
Sc	4	1	<1	<1	8	<1	<1	<1
Ba	112	80	146	80	104	151	147	99
Be	<1	6	2	4	<1	<1	4	3
Co	0.8	0.7	0.3	0.8	1.3	1.2	1.6	9.2
Cs	2.1	1.2	<0.1	0.6	0.2	0.2	0.6	<0.1
Ga	18.1	16	12.7	14.4	17.6	12.4	14.5	8.7
Hf	0.3	1.9	1.4	1.6	0.3	0.3	1.8	0.8
Nb	16.7	45.9	30.8	52.9	39.9	6.4	6.4	14.8
Rb	150.1	25.1	13.4	35.8	4.1	2.9	13	1.2
Sn	5	<1	1	<1	1	<1	<1	<1
Sr	20	68.6	65.5	47.1	88.4	257.4	2842.8	208.8
Ta	1.1	3.2	2.3	4	1.5	0.8	0.8	1.3
Th	0.7	2.4	3.8	2.7	0.4	0.8	2.4	1.3
U	0.8	1.6	2.4	9.2	0.7	1	2.2	1.2
V	<8	<8	<8	<8	9	<8	<8	<8
W	1.4	0.6	0.7	<0.5	1	<0.5	<0.5	<0.5
Zr	5.2	32.8	23.5	19.7	3.5	5.1	34.3	18.3
Y	5.4	21.9	25.9	23.5	4	7.6	7.6	7.7
La	1.7	7	7.2	3.8	1.7	3.2	1.5	5.1
Ce	2.4	12.6	14.5	7.7	2.5	5	2	7.2
Pr	0.19	1.41	1.7	0.88	0.29	0.51	0.3	0.69
Nd	0.8	4.8	6.7	4.3	1.1	1.8	1	2.3
Sm	0.29	1.48	1.74	1.79	0.38	0.56	0.53	0.71
Eu	0.02	0.1	0.02	0.15	0.06	0.04	0.24	0.14
Gd	0.41	1.98	2.54	2.84	0.34	0.71	0.61	0.87
Tb	0.11	0.44	0.55	0.68	0.1	0.17	0.16	0.19
Dy	0.73	3.29	3.95	4.3	0.59	1.16	0.97	1.22
Ho	0.15	0.65	0.79	0.72	0.12	0.29	0.22	0.24
Er	0.64	1.84	2.63	2.13	0.34	0.82	0.6	0.89
Tm	0.08	0.3	0.36	0.37	0.06	0.13	0.11	0.13
Yb	0.55	2.27	2.51	2.39	0.56	0.81	0.84	0.83
Lu	0.09	0.34	0.37	0.36	0.08	0.13	0.16	0.12
Cu	5.7	1.7	3	3.7	4.6	2.8	6.6	2.1
Pb	12.3	3.4	4.2	2.7	0.6	2.1	1.5	1.4
Zn	2	3	2	2	2	1	<1	1
Ni	2.2	1.7	5	5.6	10	6.1	3.8	22.2
La/Sm	5.86	4.72	4.13	2.12	4.47	5.71	2.83	7.18
La_N	5.48	22.58	23.23	12.26	5.48	10.32	4.84	16.45
Yb_N	2.63	10.86	12.01	11.44	2.68	3.88	4.02	3.97
$(La/Yb)_N$	2.08	2.08	1.93	1.07	2.05	2.66	1.20	4.14
La/Yb	3.09	3.08	2.87	1.59	3.04	3.95	1.79	6.14
Sr/Y	3.70	3.13	2.53	2.00	22.10	33.87	374.05	27.12
Rb/Sr	7.51	0.37	0.20	0.76	0.05	0.01	0.00	0.01
Rb/Ba	1.34	0.31	0.09	0.45	0.04	0.02	0.09	0.01
Mg#	28.53	44.60	47.67	34.32	35.58	69.57	61.55	75.20
Σ REE	8.16	38.5	45.56	32.41	8.22	15.33	9.24	20.63
Eu/Eu*	0.18	0.18	0.03	0.2	0.51	0.19	1.29	0.54
ASI	1.176	1.123	1.067	1.039	1.041	1.022	1.026	0.972

ASI: aluminium saturation index calculated with GCDkit-software (Janousek et al., 2006) as molar $Al_2O_3/(CaO+Na_2O+K_2O)$ vs. molar $Al_2O_3/(Na_2O+K_2O)$.

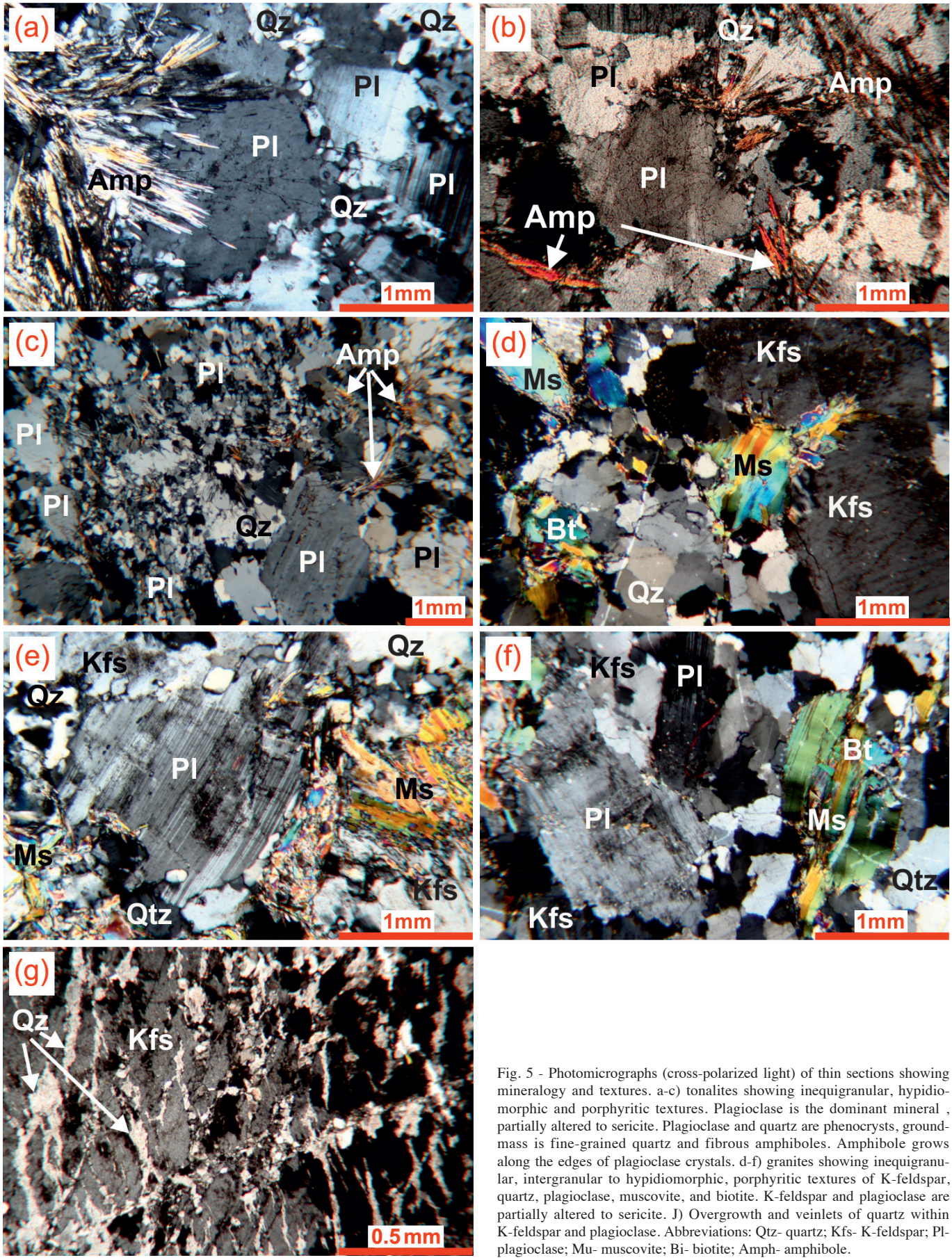

Fig. 5 - Photomicrographs (cross-polarized light) of thin sections showing mineralogy and textures. a-c) tonalites showing inequigranular, hypidiomorphic and porphyritic textures. Plagioclase is the dominant mineral , partially altered to sericite. Plagioclase and quartz are phenocrysts, groundmass is fine-grained quartz and fibrous amphiboles. Amphibole grows along the edges of plagioclase crystals. d-f) granites showing inequigranular, intergranular to hypidiomorphic, porphyritic textures of K-feldspar, quartz, plagioclase, muscovite, and biotite. K-feldspar and plagioclase are partially altered to sericite. J) Overgrowth and veinlets of quartz within K-feldspar and plagioclase. Abbreviations: Qtz- quartz; Kfs- K-feldspar; Pl- plagioclase; Mu- muscovite; Bi- biotite; Amph- amphibole.

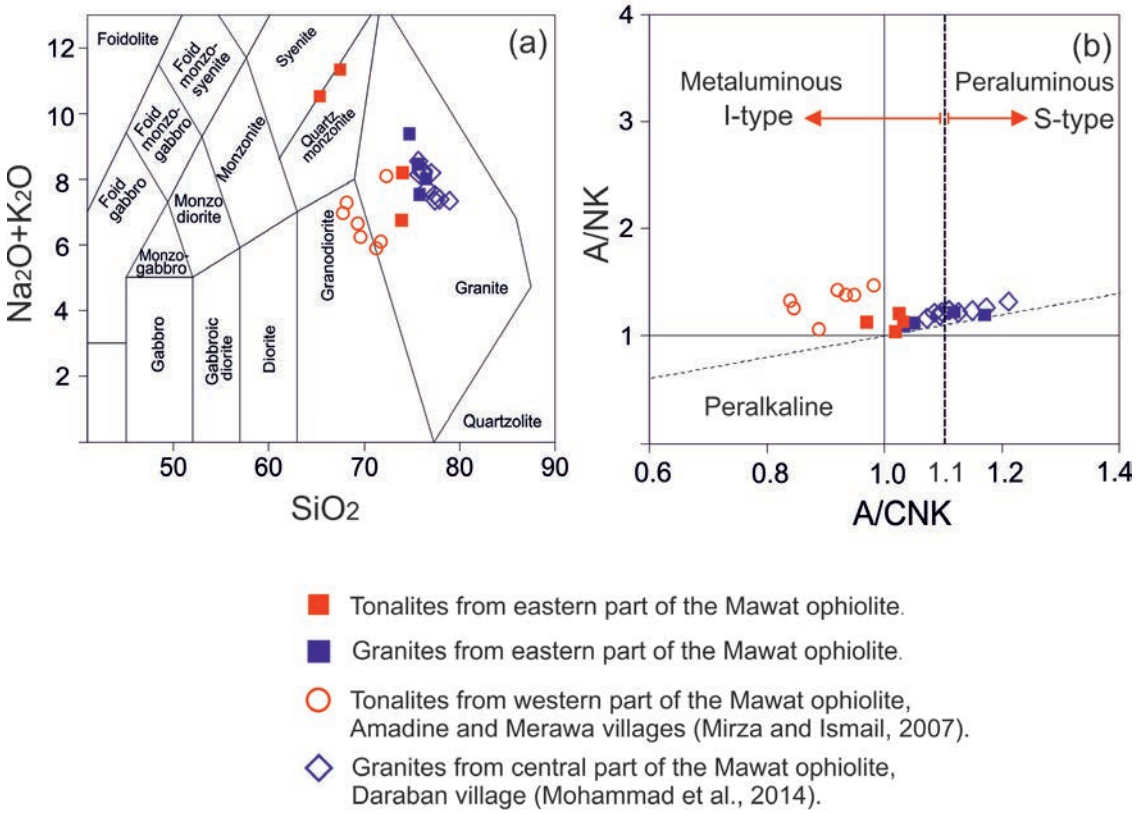

Fig. 6 - Classification diagrams: a) Total Alkali vs. Silica (TAS) diagram (Middlemost, 1994); b) A/CNK ((Al_2O_3/(CaO + Na_2O + K_2O)) vs. A/NK (Al_2O_3/(Na_2O + K_2O)).

CaO (0.14 - 0.61 wt%) contents. The Al_2O_3 contents are 13.7 - 14.34 wt%. They are classified as granites in the TAS diagram (Fig. 6a). Their ASI values range between 1.03-1.17 (peraluminous; Fig. 6b). K_2O content is highly variable (Fig. 7f). The samples from central Mawat plot in the same fields as the Type-2 samples of this study.

Trace elements

Tonalites

The REE patterns show low to moderate LREE enrichment and flat to slightly concave-up in HREE. The ΣREE abundance is low (8.22-20.63 ppm), and the rocks display a weak LREE-enrichment relative to HREE [$(La/Yb)_N$ = 1.20-4.14] with negative Eu anomalies (Eu/Eu* = 0.19 - 0.54), except one sample (19G) that shows positive anomaly (Eu/Eu* = 1.29). The REEs from Gd to Dy are slightly depleted compared to Yb and Lu in the eastern dykes. Samples from western Mawat show steeper REE pattern with higher LREE and lower HREE (Fig. 8a). The eastern tonalites are low in Ni and extremely low in Cr and V compared to the western tonalites (Table 1; Fig. 9k and l).

In the multi-element diagram (Fig. 8b), the eastern tonalites show negative anomalies for the high field strength elements (HFSEs) Ti and P, weak depletion in large ion lithophile elements (LILEs) such as Rb, Th, and K, and enrichment in Cs, Ba, U, Pb, and Sr. Sr exhibits high values (88-257 ppm) and is anomalously high in sample 19G (2842 ppm; Fig. 9a). Low Y (4-7.7 ppm) contents (Fig. 9b) and moderately high Sr/Y (22.1-374; Table 1, Fig. 11) are observed. The samples from western Mawat have consistently very high Sr contents (> 700 ppm), low Y (< 14 ppm; Fig. 9a and b) and high Sr/Y (> 64; Fig. 11).

Granites

The REE patterns show slight LREE-enrichment [$(La/Yb)_N$ = 1.07-2.08] and flat MREE to HREE with very slight MREE depletion and pronounced negative Eu anomalies (Eu/Eu* = 0.03-0.20; Table 1; Fig. 8c). In the multi-element diagram (Fig. 8d), the eastern granite samples are enriched in Cs, Rb, K, Pb, U, and Nb, and they are depleted in Ba, Sr, Ti, and Zr. These granites have low to moderate ΣREE content (8.16-45.56 ppm), and the LILEs display large variations in Rb (13.4-150.1 ppm), Ba (80-146 ppm), Zr (5.2-32.8 ppm) and Th (0.7-3.8 ppm) contents (Fig. 9). the central Mawat samples have REE patterns resembling those of the eastern MO granites. They have LREE-enrichment and flat HREE with negative Eu anomalies (Fig. 8c). Some samples are enriched in incompatible trace elements such as Ba, Rb, K and Nb, and are depleted in Sr and Ti (Fig. 8d).

DISCUSSION

Magma sources of the felsic rocks

Since the felsic rocks fall into two groups, the tonalites, and granites, their magma sources might be different. The Rb/Sr vs. Rb/Ba diagram (Fig. 10a) differentiates the magma sources and suggests that the tonalites and granites derive from mafic and sedimentary sources, respectively. The low K_2O and Rb (Figs. 7f and 9d), in particular, support a mafic source for the tonalites (Rollinson, 2014). The high K, Rb, Th, U, and Pb in the granites along with the aluminous mineralogy suggests that they formed through partial melting of metasediments. (Cox et al., 1999; Rollinson, 2014; Haase et al., 2015; Fig. 8d).

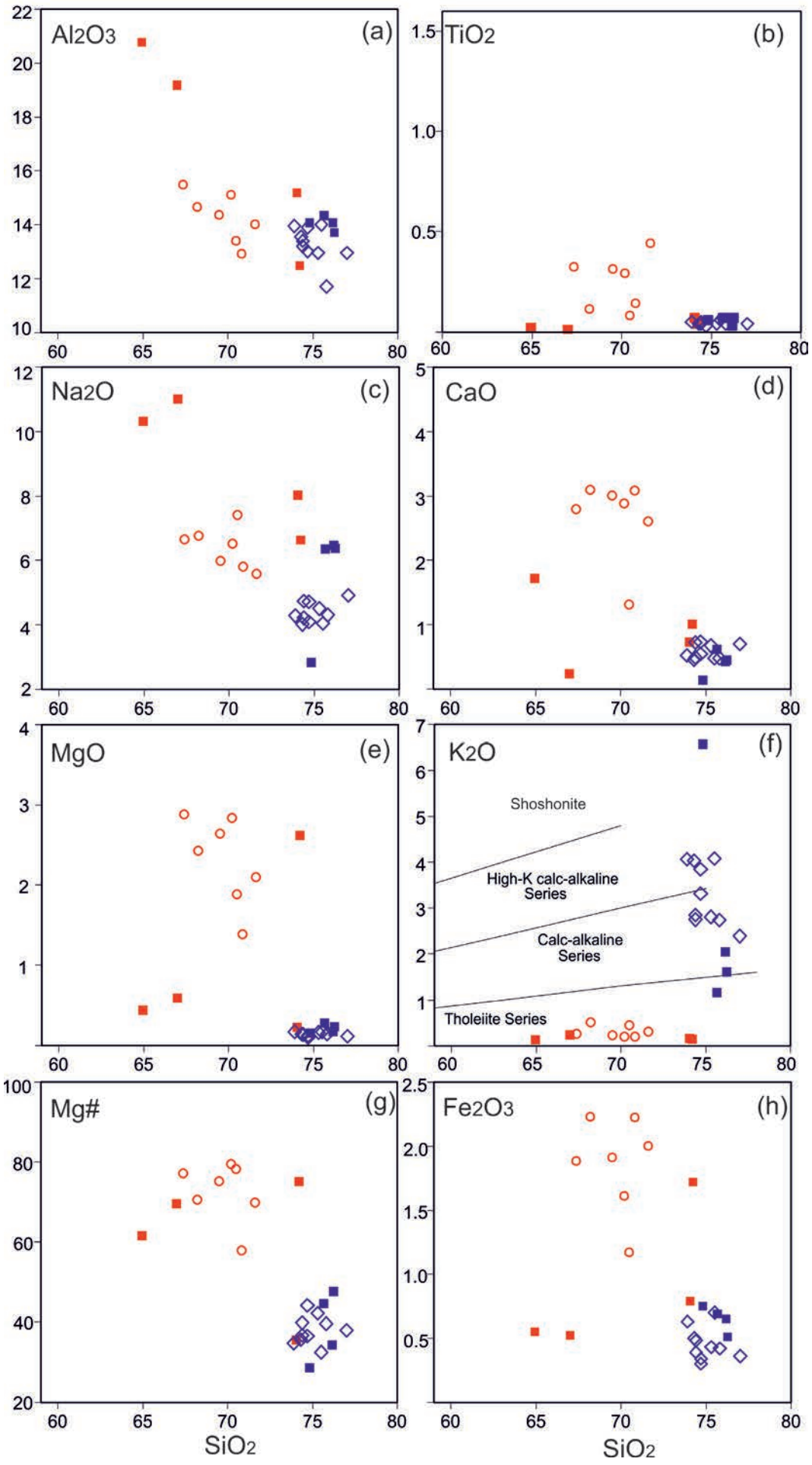

Fig. 7 - Selected major element vs. silica diagrams. f) K_2O vs. SiO_2 classification after Peccerillo and Taylor (1976) and g) Mg# = (100*MgO/(FeO_t + MgO)). All the values are in weight % except Mg#. Symbols as in Fig. 6.

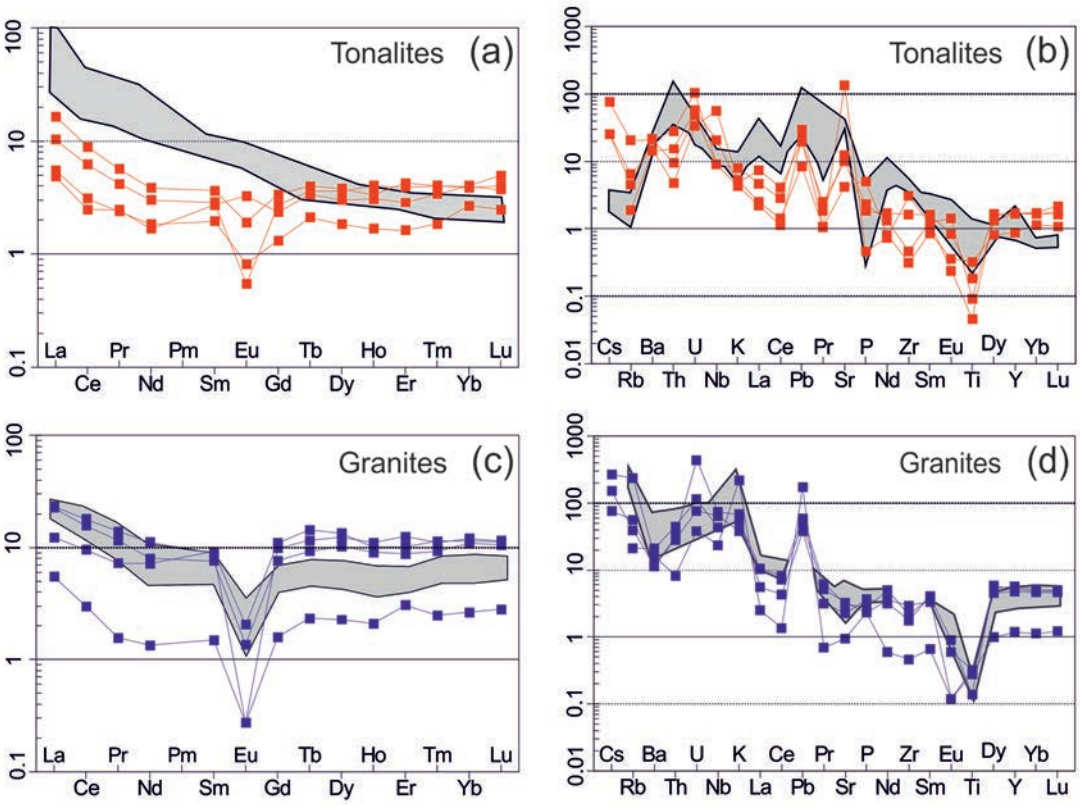

Fig. 8 - Chondrite-normalized (Boynton, 1984) REE-diagrams for: a) tonalites (western tonalities, Mirza and Ismail, 2007) shown with grey shaded field); c) granites; (central granites,(Mohammad et al., 2014) shown with grey shaded field). Primitive mantle-normalized (Sun and McDonough, 1989) multi-element diagrams for: b) tonalites (western tonalites, Mirza and Ismail, 2007) shown with grey shaded field); d) granites (central granites, Mohammad et al., 2014) shown with grey shaded field).

Tonalites

As the MO tonalites are interpreted to derive from a mafic source, the next step is to define the process involved. Two processes are possible: extreme fractional crystallization of mafic magma or anatexis of a mafic source. The melt obtained by partial melting of a mafic source is characterizsed by low K_2O and Rb contents (Rollinson, 2014), which is consistent with the eastern and western tonalites compositions (Figs. 7f and 9d). Also, the low to high La/Sm ratio for a given La concentrations (Fig. 10c) implies that these trace elements are more likely to be controlled by partial melting rather than fractional crystallization. The western tonalites show an adakitic signature (Fig. 11; Mirza and Ismail 2007), suggesting partial melting of a mafic source at high-pressure conditions.

The incompatible trace elements such as Zr and Y can effectively distinguish the processes of partial melting and fractional crystallization (Pedersen and Malpas, 1984). In the Zr vs. Y diagram, the eastern and western tonalites plot in the field of the anatectic melting which define a partial melting of a mafic source (Karmoy-type; Fig. 10b).

Eastern tonalites have low concentrations of U, Th, Rb, Ta, Ce, and La (Fig. 9). However, some of these trace elements such as U, Th, and La are in the range of the central granites (Fig. 9f, g. and h). This may suggest that sediment-derived melts were also partially involved.

The zircon ε_{Hf} data reported from the eastern tonalite sample 19G show a range of initial ε_{Hf} values (-4.4 to -1.7; Al Humadi et al., 2019). The negative ε_{Hf} values require an additional component of non-radiogenic Hf to be present in the magmas, which strongly points to continental material (c.f., Griffin et al., 2000). Hf isotope composition thus indicates that the eastern tonalites were likely derived from mixed sources or were contaminated with sediments.

As discussed above, the western tonalites were formed by the partial melting of a mafic source (Mirza and Ismail, 2007; Fig. 10a). The concentrations of Th, La, and Ce (Fig. 9g, h and i) are typical of a continental crust and therefore suggest that the mafic-derived melt were contaminated by crustal components.

As a whole, the eastern and western tonalites show similar compositions but also differ in some important aspects. The western tonalites show high Sr and low Y and Yb (< 8 and 0.9 ppm, respectively; Fig. 9) leading to high Sr/Y (145-333) and the samples plot in the adakite field (Fig. 11). They also have high MgO, Mg#, Ni and V suggesting that they were contaminated within the mantle wedge (c.f., Oman mantle section plagiogranites; Rollinson, 2014). These features are consistent with adakitic melts derived from subducted oceanic slab (Defant and Drummond, 1990; Martin, 1999). The eastern tonalites have similarly low Y and Yb contents but Sr contents lower than the western ones. Therefore, their Sr/Y are lower (22-34 ppm with one outlier 374 ppm) and they straddle the adakite/volcanic arc boundary in Fig. 11. As the eastern tonalites derive from mixtures of mafic and felsic magmas, the low Sr sedimentary component may have lowered the Sr/Y ratio. However, the effect cannot be that drastic as shown between the western and eastern samples. Secondary enrichment in mobile Sr could explain the anomalously high Sr of sample 19G (2843 ppm; Fig. 9a). The low Y and Yb show that the melting has occurred at high pressure in the garnet stability field as those elements have high distribution coefficients (K_D) in garnet (Rollinson, 1993). The eastern tonalites also have low Mg, Ni, Co and V contents (except sample 23G with high MgO 2.62 wt%) and negligible Cr (below detection limit). On the other hand, Mg# are similar in both locations (Fig. 7g). Our interpretation is that the eastern tonalite magma fractionated in a shallow-level andesitic magma chamber. Hornblende has very high K_D for Co, Cr, Ni and V in andesitic magma (Rollinson, 1993) and fractionates together with plagioclase (Moyen, 2009). Low concentration of these elements may be therefore related to hornblende (+ plagioclase) removal.

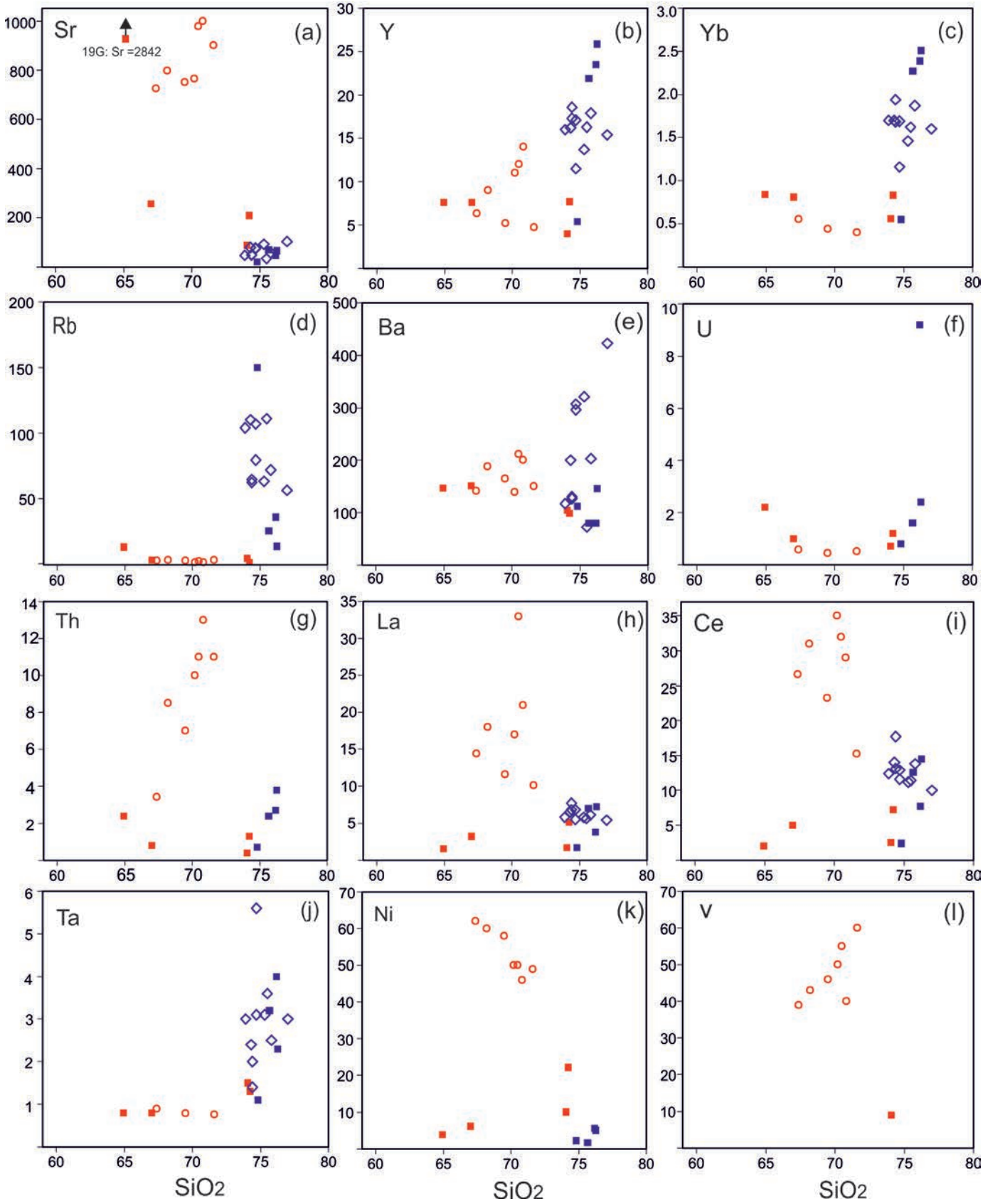

Fig. 9 - Selected trace element vs. SiO_2 diagrams. All values are in ppm. Symbols as in Fig. 6.

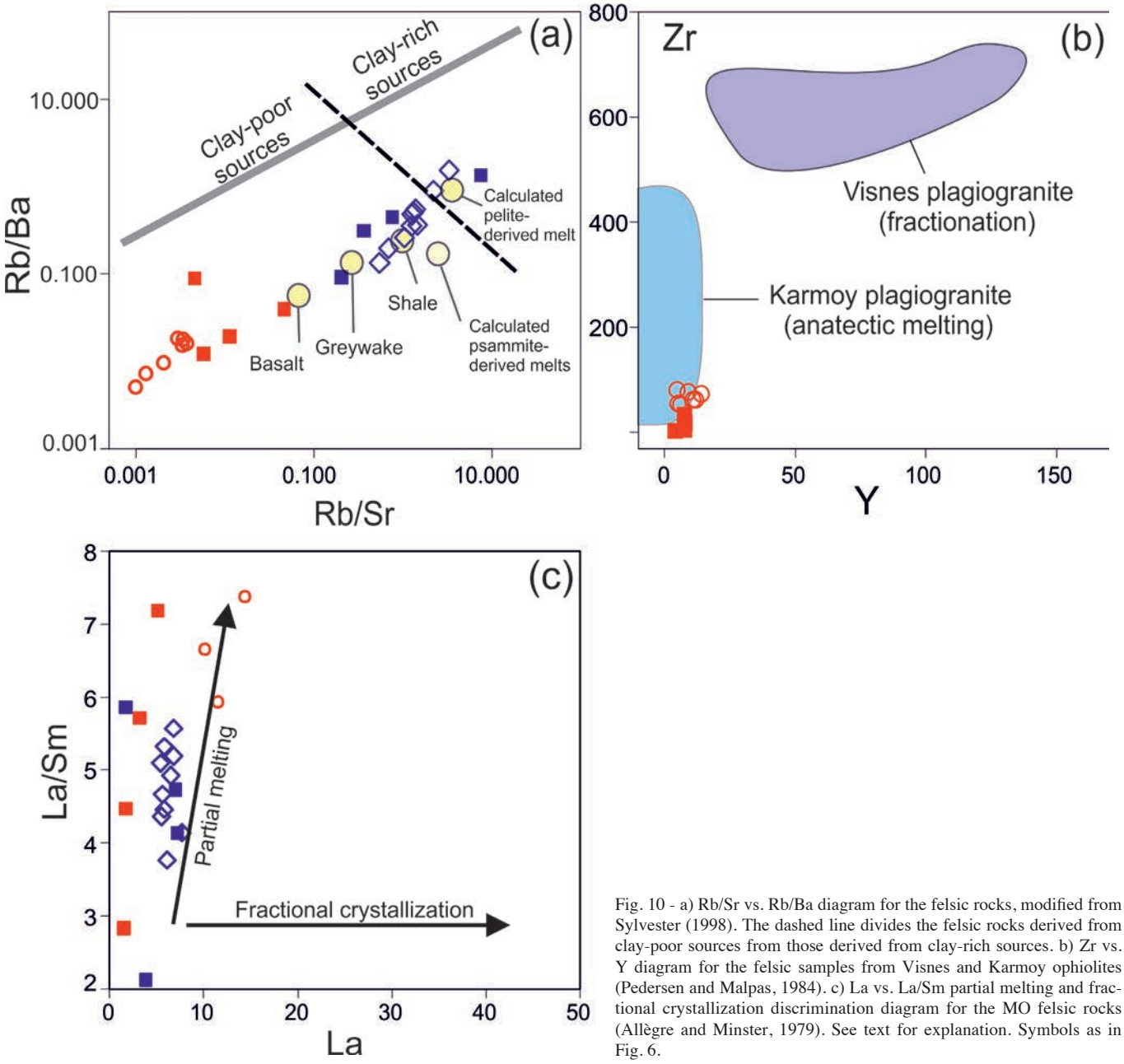

Fig. 10 - a) Rb/Sr vs. Rb/Ba diagram for the felsic rocks, modified from Sylvester (1998). The dashed line divides the felsic rocks derived from clay-poor sources from those derived from clay-rich sources. b) Zr vs. Y diagram for the felsic samples from Visnes and Karmoy ophiolites (Pedersen and Malpas, 1984). c) La vs. La/Sm partial melting and fractional crystallization discrimination diagram for the MO felsic rocks (Allègre and Minster, 1979). See text for explanation. Symbols as in Fig. 6.

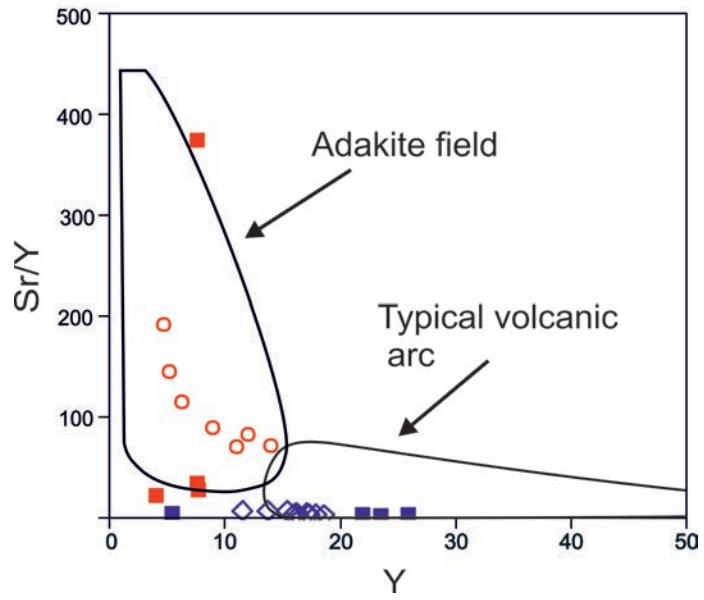

Fig. 11 - Sr/Y vs. Y diagram after Defant and Drummond (1990). Symbols as in Fig. 6.

Granites

A special feature of the granites is the low contents of REEs and LILEs; in particular, LREEs are lower than in most granites which are commonly characterized by steeper REE patterns (e.g., Guo and Wilson, 2012). The dykes show nearly flat REE patterns with very small LREE enrichment and a prominent negative Eu anomaly (Fig 8c, d).

The low LREE contents point to low contents of minerals in the source carrying these elements, mostly micas. As shown, e.g., by Condie (1993), psammitic sources such as sandstones and volcanic detritus are low in REEs and, therefore, are the most likely candidates. This is fully compatible with the Rb/Ba and Rb/Sr diagram in Fig. 10a which shows that the granites may have crystallized from metapsammite- and metagreywacke-derived melts, except sample 17G that plot in the metapelite field. The psammite-derived melts tend to have higher Rb/ Sr and Rb/Ba than their source. Thus, the Rb/Sr and Rb/Ba of the granite melts reflect not only the source composition but also the amount of feldspars left behind in the source (e.g., Harris and Inger, 1992).

In addition, several lines of evidence indicate mineral fractionation. The most obvious is the prominent negative Eu anomaly in the REE patterns, which relates to plagioclase fractionation. The negative Ba, Sr, Nb, P and Ti anomalies in the multi-element variation diagrams (Fig. 8d) are consistent with fractionation of Ti- bearing phases (e.g., ilmenite and titanite) and K-feldspar (e.g., Healy et al., 2004; Deschamps et al., 2018). Overall, partial melting of psammitic source rocks combined with fractional crystallisation may have eventually produced the flat REE pattern with negative Eu anomaly.

The initial ε_{Hf} values from zircons from sample D3/G fall in the range from -10.0 to +2.2 (Al Humadi et al., 2019). These values indicate that the source of the granite melts have a variable contribution from an old crustal component. The wide range of these values suggest heterogeneous and/or mixed sources.

The exact source region for these granites is not as clearly defined as for the tonalites. The low and widely ranging zircon initial ε_{Hf} values suggest a much older and heterogeneous source. The psammitic low REE protoliths could have several sources of different ages. Mixing with tonalitic magmas should not be able to significantly lower the ε_{Hf} values because of the relatively young age of the tonalite source. The Red Bed Series, onto which the MO was thrust (Fig. 3), is a possible candidate. However, the majority of the detrital zircons in these sandstones are from 37 to 60 Ma old (Koshnaw et al., 2018) showing that these rocks had not yet been deposited when the 95 Ma dykes intruded.

We propose that the most likely source is represented by the subducted sediments from the accretionary prism formed in a fore-arc basin (Mohammad and Qaradaghi, 2016). In such environment, sediments from several sources are deposited and felsic material from eroded continents and volcanic arcs are common (e.g., Cawood et al., 2009). By continued subduction, the subducted sediments on top of the mafic oceanic crust melt by heat from the hot mantle wedge above. This model was applied to the Oman mantle section granitoid dykes by Rollinson (2015) who concluded that both subducted oceanic slab and the sediments on top of the slab were simultaneously melted and mixed. In the Oman example, the melts interacted with the mantle wedge. The Mawat granites are low in MgO, Ni and Cr and do not favour this interpretation. However, the Wadi Fizh and Al Dadnah granites in Oman also are low in these elements and the REE patterns in Al Dadnah are very similar to the Mawat ones. The low contents of compatible elements can be explained by the large volume of melt in the central granites leading to high melt/rock ratio and low contamination degree (Moyen, 2009). In the eastern granites hornblende fractionation in a shallow-level magma chamber may have removed those elements. The hornblende fractionation was interpreted for the eastern tonalites and because the magmas are mixed the same idea can be extended to the granites as well.

CONCLUSIONS

Felsic dykes are found in the western, central and eastern parts of the Mawat ophiolite. They occur in two compositional groups; tonalites and granites.

The western dykes are tonalites and show high Sr/Y ratios, high MgO and Ni contents and resemble adakitic melts derived from subducted oceanic crust contaminated by mantle wedge peridotites. The central dykes are granites derived from a sedimentary source

The eastern dykes include both tonalites and granites. They are mixed with each other in various proportions and have intermediate compositions between western and central dykes.

The eastern tonalites have lower MgO, Cr and Ni contents and lower Sr/Y than the western ones. They are interpreted to be formed by hornblende and plagioclase fractionation in a shallow-level magma chamber. Hornblende fractionation is also suggested as responsible for the low Mg, Cr and Ni contents in the granites.

The eastern granites are high in K_2O, Rb and LREEs and are derived from subducted sediments.

ACKNOWLEDGMENTS

This study was funded by the Ministry of Higher Education and Scientific Research of Iraq (grant No. 33630/2014), University of Babylon, Iraq, and the Department of Geography and Geology, University of Turku, Finland. Arto Peltola is thanked for making the polished thin sections. The manuscript was much improved by constructive comments and suggestions by two anonymous reviewers. This is a Finnish Geosciences Research Laboratory contribution.

REFERENCES

Agard P., Omrani J., Jolivet L. and Mouthereau F., 2005. Convergence history across Zagros (Iran): constraints from collisional and earlier deformation. Int. J. Earth Sci., 94: 401-419.

Alavi M., 1980. Tectonostratigraphic evolution of the Zagrosides of Iran. Geology, 8: 144-149. https://doi.org/10.1130/0091-7613(1980)8<144:TEOTZO>2.0.CO;2

Alavi, M. 2008. Structures of the Zagros Fold-Thrust Belt in Iran. Am. J. Sci., 308, 104-104. https://doi.org/10.2475/01.2008.05

Al Humadi H., Väisänen M., Ismail S.A., Kara J., O'Brien H., Lahaye Y. and Lehtonen M., 2019. U-Pb geochronology and Hf isotope data from the Late Cretaceous Mawat ophiolite, NE Iraq. Heliyon, 5; e02721. https://doi.org/10.1016/j.heliyon.2019.e02721.

Ali S.A., Buckman S., Aswad K.J., Jones B.G., Ismail S.A. and Nutman A.P., 2012. Recognition of Late Cretaceous Hasanbag ophiolite-arc rocks in the Kurdistan Region of the Iraqi Zagros suture zone: A missing link in the paleogeography of the closing Neotethys Ocean. Lithosphere, 4: 395-410.

Ali S.A., Buckman S., Aswad K.J., Jones B.G., Ismail S.A. and Nutman A.P., 2013. The tectonic evolution of a Neo-Tethyian (Eocene-Oligocene) island-arc (Walash and Naopurdan groups) in the Kurdistan region of the Northeast Iraqi Zagros Suture Zone. Island Arc, 22: 104-125.

Al-Kadhimi J.A.M., Sissakian V.K., Fattah A.S. and Deikran D.B., 1996. Tectonic map of Iraq, Geol. Surv. Mining Iraq, 38 pp.

Allègre C.J. and Minster J.F., 1978. Quantitative models of trace element behavior in magmatic process. Earth Planet. Sci. Lett., 38: 1-25.

Al-Mehaidi H. M., 1974. Geological investigation of Mawat, Chwarta area, Northeatern Iraq. Unpubl. report, SOM Library, No. 609.

Al-Qayim B., Ibrahim A. and Koyi H., 2012. Tectonostratigraphic overview of the Zagros Suture Zone, Kurdistan, NE Iraq. GeoArabia, 17: 109-15.

Amri I., Benoit M. and Ceuleneer G., 1996. Tectonic setting for the genesis of oceanic plagiogranites: evidence from a paleospreading structure in the Oman ophiolite. Earth Planet. Sci. Lett., 139: 177-194.

Arai S., Shimizu Y., Ismail S.A. and Ahmed A.H., 2006. Low-T formation of high-Cr spinel with apparently primary chemical characteristics within podiform chromitite from Rayat, northeastern Iraq. Miner. Mag., 70: 499-508.

Aziz N.R.H., 2008. Petrogenesis, evolution, and tectonics of the serpentinites of the Zagros Suture Zone, Kurdistan Region, NE Iraq. Unpubl. Ph. D. Thesis, Univ. Sulaimani, 250 pp.

Azizi H., Hadi A., Asahara Y. and Mohammad Y.O., 2013. Geochemistry and geodynamics of the Mawat mafic complex in the Zagros Suture Zone, northeast Iraq. Cent. Eur. J. Geosci., 5: 523-537.

Boynton W.V. 1984. Cosmochemistry of the rare earth elements: meteorite studies. In: R. Henderson (Ed.), Rare Earth element geochemistry. Develop. Geochem., Elsevier, 2: 63-114.

Buday T. and Jassim S.Z., 1987. Tectonism, magmatism and metamorphism. The regional geology of Iraq, Geol. Surv. Iraq, 2, 352 pp.

Cawood P.A., Kröner A., CollinsW.J., Kusky T.M., Mooney W.D. and Windley B.F., 2009. Accretionary orogens through Earth history. J. Geol. Soc., 318: 1-36.

Coleman R.G. and Peterman Z., 1975. Oceanic plagiogranite. J. Geophys. Res., 80: 1099-1108.

Condie K.C., 1993. Chemical composition and evolution of the upper continental crust: contrasting results from surface samples and shales. Chem. Geol., 104: 1-37.

Cox J., Searle M. and Pedersen R., 1999. The petrogenesis of leucogranitic dykes intruding the northern Semail ophiolite, United Arab Emirates: field relationships, geochemistry and Sr/Nd isotope systematics. Contrib. Miner. Petrol., 137: 267-287.

Defant M.J. and Drummond M.S. 1990. Derivation of some modern arc magmas by melting of young subducted lithosphere. Nature, 347: 662-665.

Deschamps F., Duchêne S., de Sigoyer J., Bosse V., Benoit M. and Vanderhaeghe O., 2018. Coeval mantle-derived and crust-derived magmas forming two neighbouring plutons in the Songpan Ganze accretionary orogenic wedge (SW China). J. Petrol., 58: 2221-2256.

Dilek Y. and Delaloye M., 1992. Structure of the Kızıldağ ophiolite, a slow-spread Cretaceous ridge segment north of the Arabian promontory. Geology, 20: 19-22

Dilek Y. and Furne H., 2014. Ophiolites and their origins. Elements, 10: 93-100.

Dilek Y. and Furnes H., 2017. Geochemical characterization of intermediate to silicic rocks in the global ophiolite record. Acta Geol. Sinica, English Ed., 91: 8-9.

Dilek Y. and Furnes H., 2019. Tethyan ophiolites and Tethyan seaways. J. Geol. Soc., 176: 899-912.

Dilek Y. and Moores E.M., 1990. Regional tectonic of the eastern Mediterranean ophiolites. In: J. Malpas, E.M. Moores, A. Panayiotou and C. Xenophontos (Eds.), Ophiolites, oceanic crustal analogues. Proceed. Symp. 'Troodos 1987'. Geol. Surv. Dept., Nicosia, Cyprus, p, 295-309.

Dilek Y. and Thy P., 2009. Island arc tholeiite to boninitic melt evolution of the Cretaceous Kizildag (Turkey) ophiolite: model for multi-stage early arc–forearc magmatism in Tethyan subduction factories. Lithos, 113: 68-87.

Dilek Y., Furnes H. and Shallo M., 2007. Suprasubduction zone ophiolite formation along the periphery of Mesozoic Gondwana. Gondw. Res., 11: 453-475.

Dixon S. and Rutherford M.J., 1979. Plagiogranites as late-stage immiscible liquids in ophiolite and mid-ocean ridge suites: an experimental study. Earth Planet. Sci. Lett., 45: 45-60. https://doi.org/10.1016/0012-821X(79)90106-

Flagler P.A. and Spray J.G., 1991. Generation of plagiogranite by amphibolite anatexis in oceanic shear zones. Geology, 19: 70-73.

Floyd P.A., Yaliniz M.K. and Göncüoğlu M.C., 1998. Geochemistry and petrogenesis of intrusive and extrusive ophiolitic plagiogranites, Central Anatolian Crystalline Complex, Turkey. Lithos, 42: 225-41. https://doi.org/10.1016/S0024-4937(97)00044-3

France L., Ildefonse B. and Koepke J., 2009. Interactions between magma and hydrothermal system in Oman ophiolite and in IODP Hole 1256D: Fossilization of a dynamic melt lens at fast spreading ridges. Geochem. Geophys. Geosyst. https://doi.org/10.1029/2009GC002652

France L., Koepke J., Ildefonse B., Cichy S.B. and Deschamps F., 2010. Hydrous partial melting in the sheeted dike complex at fast spreading ridges: experimental and natural observations. Contrib. Miner. Petrol., 160: 683-704.

Freund S., Haase K.M., Keith M., Beier C. and Garbe-Schönberg D., 2014. Constraints on the formation of geochemically variable plagiogranite intrusions in the Troodos Ophiolite, Cyprus. Contrib. Miner. Petrol., 167: 1-22.

Gerlach D.C., Leeman W.P. and Lallemant H.G.A. 1981. Petrology and geochemistry of plagiogranite in the Canyon Mountain Ophiolite, Oregon. Contrib. Miner. Petrol., 77: 82-92. https://doi.org/10.1007/BF01161505

Griffin W.L., Pearson N.J., Belousova E., Jackson S.V., Van Achterbergh E., O'Reilly S.Y. and Shee S.R., 2000. The Hf isotope composition of cratonic mantle: LAM-MC-ICPMS analysis of zircon megacrysts in kimberlites. Geochim. Cosmochim Acta, 64: 133-147.

Grimes C.B., Ushikubo T., Kozdon R. and Valley W., 2013. Perspectives on the origin of plagiogranite in ophiolites from oxygen isotopes in zircon. Lithos, 179:48-66 https://doi.org/10.1016/j.lithos.2013.07.026

Guo Z. and Wilson M., 2012. The Himalayan leucogranites: constraints on the nature of their crustal source region and geodynamic setting. Gondw. Res., 22: 360-376.

Haase K.M., Freund S., Koepke J., Hauff F. and Erdmann M., 2015. Melts of sediments in the mantle wedge of the Oman ophiolite. Geology, 43: 275-278.

Harris N.B.W. and Inger S., 1992. Trace element modelling of pelite-derived granites. Contrib. Miner. Petrol., 110: 46-56.

Healy B., Collins W.J. and Richards S.W., 2004. A hybrid origin for Lachlan S-type granites: the Murrumbidgee Batholith example. Lithos, 78: 197-216.

Ismail S.A. and Al-Chalabi S.A., 2006. Genesis of chromitite in Qalander Area, northern Iraq, employing Cr-rich spinel. J. Kirkuk Univ., Scientific Studies, 1: 10-29.

Ismail S.A. and Carr P.F.A., 2008. Brief review of ophiolites in Iraq. Proceed. Intern. Symp. Geoscience Resources and Environments of Asian Terranes, 4th IGCP 516, and 5th APSEG; November 2008, p. 60. Bangkok, Thailand. Abstruct Book.

Ismail S.A., Ali A., Nutman A.P., Bennett V.C. and Jones B.G., 2017. The Pushtashan juvenile suprasubduction zone assemblage of Kurdistan (northeastern Iraq): A Cretaceous (Cenomanian) Neo-Tethys missing link. Geosci. Front., 8: 1073-1087.

Ismail S.A., Arai S., Ahmed A.H. and Shimizu Y., 2009. Chromitite and peridotite from Rayat, northeastern Iraq, as a fragment of Tethyan ophiolite. Island Arc, 18: 175-183.

Ismail S.A., Kettanah Y.A., Chalabi S.N., Ahmed A.H. and Arai S., 2014. Petrogenesis and PGE distribution in the Al-and Cr-rich chromitites of the Qalander ophiolite, northeastern Iraq: Implications for the tectonic environment of the Iraqi Zagros Suture Zone. Lithos, 202: 21-36.

Ismail S.A., Koshnaw R.I., Barber D.E., Al Humadi H. and Stockli D.F., 2020. Generation and exhumation of granitoid intrusions in the Penjween ophiolite complex, NW Zagros of the Kurdistan region of Iraq: Implications for the geodynamic evolution of the Arabian-Eurasian collision zone. Lithos, 376, 105714.

Ismail S.A., Mirza T.M. and Carr P.F., 2010. Platinum-group elements geochemistry in podiform chromitites and associated peridotites of the Mawat ophiolite, northeastern Iraq. J. Asian Earth Sci., 37: 31-41.

Janousek V., Farrow C.M. and Erban V., 2006. Interpretation of whole-rock geochemical data in igneous geochemistry: introducing Geochemical Data Toolkit (GCDkit). J. Petrol., 47: 1255-1259.

Jassim S.Z., 1973. Geology of the central sector of the Mawat Igneous Complex, Northeastern Iraq. J. Geol. Soc. Iraq, 5: 83-92.

Jassim S.Z. and Goff J.C., 2006. Geology of Iraq. Brno, Czech Republic, Dolin, Prague and Moravian Museum, 341 pp.

Koepke J., Berndt J., Feig S.T. and Holtz F., 2007. The formation of SiO_2-rich melts within deep oceanic crust by hydrous partial melting of gabbros. Contrib. Miner. Petrol., 153: 67-84.

Koepke J., Feig S.T., Snow J. and Freise M., 2004. Petrogenesis of oceanic plagiogranites by partial melting of gabbros: an experimental study. Contrib. Miner. Petrol., 146: 414-432.

Koshnaw R.I., Stockli D.F. and Schlunegger F., 2018, Timing of the Arabia-Eurasia continental collision Evidence from detrital zircon U-Pb geochronology of the Red Bed Series strata of the northwest Zagros hinterland, Kurdistan region of Iraq. Geology, 47: 47-50.

Koshnaw R.I., Horton B.K., Stockli D.F., Barber D.E and Tamar-Agha M.Y., 2019. Sediment routing in the Zagros foreland basin: Drainage reorganization and a shift from axial to transverse sediment dispersal in the Kurdistan region of Iraq. Basin Res., 32: 688-715. https://doi.org/10.1111/bre.12391

Li W.X. and Li X.H., 2003. Adakitic granites within the NE Jiangxi ophiolites, South China: geochemical and Nd isotopic evidence. Precambr. Res., 122: 29-22.

Li W.X., Li X.H., Li Z.X. and Lou F.S., 2008. Obduction-type granites within the NE Jiangxi Ophiolite: implications for the final amalgamation between the Yangtze and Cathaysia Blocks. Gondw. Res., 13: 288-301.

Malpas J., 1979. Two contrasting trondhjemite associations from transported ophiolites in Western Newfoundland: Initial report. In: Barker F. (ed) Trondhjemites, dacites, and related rocks. Elsevier, Amsterdam, pp 465-487.

Martin H., 1999. Adakitic magmas: modern analogues of Archaean granitoids. Lithos, 46: 411-429.

Maurizot P., Cluzel D., Patriat M., Collot J., Iseppi M., Lesimple S., Secchiari A., Bosch D., Montanini A., Macera P. and Davies H.L., 2020. Chapter 5. The Eocene Subduction-Obduction Complex of New Caledonia. Mem. Geol. Soc. London 51: 93-130.

Meffre, S., Falloon T.J., Crawford T.J., Hoernle K., Hauff F., Duncan R.A., Bloomer S.H. and Wright D.J., 2012. Basalts erupted along the Tongan fore arc during subduction initiation: Evidence from geochronology of dredged rocks from the Tonga fore arc and trench. Geochem. Geophys. Geosys. 13: Q12003. https://doi.org/10.1029/2012GC004335

Middlemost E.A., 1994. Naming materials in the magma/igneous rock system. Earth Sci. Rev., 37: 215-224.

Mirza T.A. and Ismail S.A., 2007. Origin of plagiogranite in the Mawat ophiolite complex, Kurdistan Region, NE Iraq. J. Kirkuk Univ., Scientific Studies, 2: 1-25.

Moghadam H.S., Zaki Khedr M., Chiaradia M., Stern R.J., Bakhshizad F., Arai S., Ottley C.J. and Tamura A., 2014. Supra-subduction zone magmatism of the Neyriz ophiolite, Iran: constraints from geochemistry and Sr-Nd-Pb isotopes. Int. Geol. Rev., 56: 1395-1412.

Mohammad Y.O. and Cornell D.H., 2017. U-Pb zircon geochronology of the Daraban leucogranite, Mawat ophiolite, Northeastern Iraq: A record of the subduction to collision history for the Arabia-Eurasia plates. Island Arc, 26. https://doi.org/10.1111/iar.12188

Mohammad Y.O. and Qaradaghi J.H., 2016. Geochronological and mineral chemical constraints on the age and formation conditions of the leucogranite in the Mawat ophiolite, Northeastern of Iraq: insight to sync-subduction zone granite. Arab. J. Geosci., 9: 1-23. https://doi.org/10.1007/s12517-016-2630-4

Mohammad Y.O., Cornell D.H., Qaradaghi J.H. and Mohammad F.O., 2014. Geochemistry and Ar-Ar muscovite ages of the Daraban Leucogranite, Mawat Ophiolite, northeastern Iraq: implications for Arabia-Eurasia continental collision. J. Asian Earth Sci., 86: 151-165.

Mouthereau F., Lacombe O. and Vergés J., 2012. Building the Zagros collisional orogen: timing, strain distribution and the dynamics of Arabia/Eurasia plate convergence. Tectonophysics, 532: 27-60.

Moyen J.F., 2009. High Sr/Y and La/Yb ratios: the meaning of the "adakitic signature". Lithos, 112: 556-574.

Pearce J.A., 1989. High T/P metamorphism and granite genesis beneath ophiolite thrust sheets. Ofioliti, 14: 195-211.

Peccerillo A. and Taylor S.R., 1976. Geochemistry of Eocene calc-alkaline volcanic rocks from the Kastamonu area, northern Turkey. Contrib. Miner. Petrol., 58: 63-81.

Pedersen R.B. and Malpas J., 1984. The origin of oceanic plagiogranites from the Karmoy ophiolite, western Norway. Contrib. Miner. Petrol., 88: 36-52.

Rollinson H.R., 1993. Using geochemistry data: Evaluation, presentation, interpretation. Longman Sci. Techn. Ltd., Essex, 352 pp.

Rollinson H., 2014. Plagiogranites from the mantle section of the Oman Ophiolite: models for early crustal evolution. Geol. Soc. London Spec. Publ., 392: 247-261.

Rollinson H., 2015. Slab and sediment melting during subduction initiation: granitoid dykes from the mantle section of the Oman ophiolite. Contrib. Miner. Petrol., 170: 1-20.

Santosh M., Teng X.M., He X.F., Tang L. and Yang Q.Y., 2016. Discovery of Neoarchean suprasubduction zone ophiolite suite from Yishui Complex in the North China Craton. Gondw. Res., 38: 1-27. https://doi.org/10.1016/j.gr.2015.10.017

Searle M.P. and Malpas J., 1980. Structure and metamorphism of rocks beneath the Semail ophiolite of Oman and their significance in ophiolite obduction. Earth Environ. Sci. Trans. the Royal Soc. Edinburgh, 71: 247-262. https://doi.org/10.1017/S0263593300013614

Sun S.S. and McDonough W.F., 1989. Chemical and isotopic systematics of oceanic basalts: implications for mantle composition and processes. In: A.D. Saunders and M.J. Norry (Eds.), Magmatism in the oceanic basin. Geol. Soc. London Spec. Publ., 42: 313-345.

Sylvester P.J., 1998. Post-collisional strongly peraluminous granites. Lithos, 45: 29-44.

Whitehead J., Dunning G.R. and Spray J.G., 2000. U-Pb geochronology and origin of granitoid rocks in the Thetford Mines ophiolite, Canadian Appalachians. Geol. Soc. Am. Bull., 112: 915-928.

Ulrich T. and Borsien J.R., 1996. Fedoz metagabbro und forno metabasalt (Val Malenco, Norditalien): Vergleichende petrographische und geochemische Untersuchungen. Schweiz. Miner. Petrogr. Mitt., 76: 521-534. https://doi.org/10.5169/seals-57713

Received, May 16, 2020
Accepted, October 7, 2020
First published online, October 23, 2020